STUDY ON THE CORRELATION ANALYSIS BETWEEN ECOLOGICAL FACTORS AND PHENOTYPIC TRAITS OF CODONOPSIS PILOSULA PLANTS AND THE DEVELOPMENT OF A 3D DYNAMIC MODEL

/

党参植株生态因子与表型相关性分析及三维动态模型构造研究

Xunhe LIU[1)], Degao ZHAO[1)], Xiaoshuan ZHANG[*1)]
[1)] College of Engineering, China Agricultural University, Beijing/China;
Tel: 010-62737663; E-mail: zhxshuan@cau.edu.cn
DOI: https://doi.org/10.35633/inmateh-78-68

Keywords: *Codonopsis pilosula (Lu Dangshen); 3D Dynamic Growth Simulation; Phenotypic Traits; Correlation Analysis; Optimal Values.*

ABSTRACT

This study focused on Codonopsis pilosula by integrating meteorological and morphological data to establish a meteorology–phenotype correlation model and a three-dimensional (3D) phenotypic structure model. Spearman correlation analysis and an improved three-way K-means clustering method were applied to investigate 3D phenotypic variation and identify correlation thresholds. Based on these analyses, a dynamic 3D growth tracking model was developed to support real-time monitoring of ecological factors and targeted agronomic interventions. Validation using measured data revealed significant relationships between environmental variables and plant growth. Specifically, a 5% increase in relative humidity at 40 cm height (15.2–22.5 °C) corresponded to an approximately 10% increase in root growth. For nitrogen content (0.6–8.0), each unit increase resulted in an approximate 8% increase in root growth. Within the temperature range of 16.94–30.81 °C, each 1 °C increase led to an approximately 7% increase in stem growth. Within the effective range of global horizontal irradiance (GHI, 255–350), each 10-unit increase resulted in a 12% increase in stem growth. For air relative humidity (ARH, 50.3–60.9%), each 5% decrease corresponded to an approximately 6% increase in leaf growth, while for phosphorus content (1.2–9.8), each unit increase led to a 9% increase in leaf growth.

摘要

本研究以山西晋城陵川县潞党参为对象，采集气象与形态数据，建立气象—表型相关模型与潞党参三维表型结构模型；采用斯皮尔曼相关与改进三支 K-means 聚类分析 3D 表型变化与相关性阈值，实现生态因子实时监测与人工干预，构建潞党参三维动态生长随动模型。实测数据检验结果表明，40cmMAT 在 15.2 到 22.5 湿度增加 5% 对应的根生长增加约 10%；N 在 0.6 到 8.0 每增加 1 个单位，对应的根生长增加约 8%；MAT 在 16.94 到 30.81 每升高 1℃，茎生长幅度提高约 7%；GHI 在 255 到 350 的正向影响区间时，每增加 10 单位时，茎生长增加 12%；ARH 在 50.3 到 60.9 每降低 5%，叶的生长增加约 6%；P 在 1.2 到 9.8 每增加 1 单位，叶生长提高 9%。

1. INTRODUCTION

Codonopsis pilosula, a plant in the *Campanulaceae* family, is widely cultivated across various regions in China *(Akhtar, 2024)*. Lu Dangshen, characterized by its sweet taste and neutral nature, is attributed to the spleen and lung meridians in traditional Chinese medicine and is known for its effects in replenishing qi, invigorating the spleen and lungs, and promoting fluid production *(Arshad, 2024)*. As a traditional Chinese medicinal herb and often referred to as the “substitute for ginseng,” *C. pilosula* is rich in bioactive compounds in its roots, such as saponins, polysaccharides, and volatile oils. These compounds exhibit significant pharmacological effects. Additionally, the market demand for *C. pilosula* remains stable, with widespread applications in the health and wellness industry, which has fueled the large-scale commercialization of its cultivation and the development of related industrial chains. Therefore, it holds substantial economic value, with its quality playing a critical role in determining its pharmacological efficacy. Analyzing the correlation between ecological factors and phenotypic traits of Lu Dangshen can indirectly assess its geoherbal authenticity, thereby determining its quality.

The study of the 3D dynamic growth structure of Lu Dangshen allows for a comprehensive analysis of the growth process and ecological structural characteristics of the herb, providing a detailed understanding of its growth, development, and phenotypic variations. Furthermore, this approach serves as a visual tool for designing cultivation systems, managing agricultural practices, and implementing artificial interventions to achieve optimal geoherbal cultivation of Lu Dangshen *(Chen, 2024)*.

Significant progress has been made in the three-dimensional reconstruction technology of plants both domestically and internationally *(Clark, 2011; Deng, 2024; Diggle, 1988)*. As early as the 1970s, Aristid Lindenmayer, the Hungarian biologist, introduced the L-system (Lindenmayer system) to describe the morphological structure of plants. Later, the French National Institute for Research in Computer Science and Automation (INRIA) proposed the reference axis technique, which defines the main and transverse axes of plants to construct 3D structural models *(Gairola, 2010)*. In 1998, Professor Philippe de Reffye of the French Agricultural Research Center (CIRAD) and Professor Wang of the Chinese Academy of Sciences jointly developed the GreenLab model, which integrates botany, mathematics, and computer science to simulate plant growth and structural formation *(Guo,2022; Jiang, 2022; Koch, 2024; Latt, 2014)*. In 2003, Professor Hu Baogang from the Chinese Academy of Sciences proposed the dual-scale automaton model, primarily used to simulate the plant growth process, particularly the development of leaves and branches *(Liang, 2024; Lu, 2024; Mohan, 2017; Murata, 2024)*.

Recent developments in plant 3D reconstruction technologies highlight both historical advancements and cutting-edge innovations. Internationally, early models like the L-system and the Reference Axis Technique laid the foundation for simulating plant morphology, while later models such as GreenLab and the Dual-Scale Automaton Model integrated interdisciplinary approaches to simulate plant growth and structure. More recently, domestic advancements, have focused on overcoming challenges related to data scarcity and complex plant structures. Re-searchers have leveraged deep learning, depth cameras, and advanced segmentation frameworks to improve 3D reconstruction, with new methods significantly enhancing the accuracy and automation of plant phenotype modeling. These developments indicate a clear trend towards more sophisticated, data-driven, and automated approaches to plant 3D reconstruction, which have broad applications in both research and industry.

Domestically, in 2023, Professor Chen's team from South China Agricultural University introduced a plant 3D reconstruction method based on depth cameras and point cloud completion using deep learning, successfully addressing the challenge of insufficient training data and effectively processing point cloud data captured by Azure Kinect *(Chen, 2023)*. In 2024, Professor Yang's team from Northwest A&F University proposed the MCAT-UNet, an efficient semantic segmentation framework based on Multi-Scale Convolution Attention (MSCA) and Cross-Window Transformation (CSWT) for automated 3D reconstruction of complex plant phenotypes *(Yang, 2024)*. The team also advanced the field by introducing a LiDAR-based approach for intelligent 3D and hyper-dimensional plant cognition *(Rahimmalek, 2017; Rodriguez, 2024; Rosell, 2009)*.

This study adopts 3D scanning and point cloud reconstruction technologies, aligning with Professor Yang Huijun's concept. The rationale is that accurate 3D model reconstruction of plants at various growth stages necessitates high fidelity to the plant's original form. While 3D scanning and point cloud reconstruction methods may appear less sophisticated compared to the techniques proposed by other scholars in the field of 3D reconstruction, these methods prove to be more suitable for ensuring experimental accuracy in representing the prototype of the plants *(Roshan, 2024; Rousseeuw, 1987; Sanzo-Miro, 2024; Sun, 2024)*.

In the field of correlation analysis, Karl Pearson proposed the Pearson product-moment correlation coefficient in 1895 to measure the linear relationship between two variables. However, due to the stringent requirements for normality and linearity, Charles Spearman introduced the Spearman's rank correlation coefficient in 1904 as an alternative for evaluating data with non-normal distributions or non-linear relationships *(Tapia, 2024)*. This method, based on the ranks of data, is particularly suited for measuring the strength of monotonic relationships. Subsequently, in the 1930s, British statistician Ronald A. Fisher developed multivariate statistical analysis methods, laying the foundation for multiple regression analysis *(Vanrell, 2024)*. Later, in the 1960s, Herman O.A. Wold introduced Partial Least Squares (PLS) regression, which further enriched the analytical tools available for multi-factor analysis *(Wold, 1966)*. In recent years, with the rapid development of big data and machine learning, Professor Li Hang has made significant progress in integrating multifactor analysis with machine learning methods, particularly in the fields of information retrieval and natural language processing.

He has conducted in-depth research in areas such as statistical learning theory, pattern recognition, and data mining, and has developed several effective algorithms and frameworks in machine learning models, especially in ensemble learning. Professor Li's research has had a substantial impact on the fields of information retrieval and natural language processing.

In the domain of clustering analysis, Budzisz in 2018 integrated three-way decision theory with the K-means algorithm, proposing a novel three-way clustering algorithm *(Budzisz, 2018; Wang, 2024; Yang, 2019)*. Subsequently, in 2023 and 2024, we applied the improved k-means three branch clustering algorithm to the optimal threshold control of temperature regulation in pig houses, which provided inspiration for this study.

While there is little controversy regarding the choice of correlation analysis methods in this study, the inherent non-linear characteristics of environmental factors and plant 3D model data make the Spearman's rank correlation coefficient more suitable for reflecting their relationships *(*Liang*, 2024)*. Therefore, this method was adopted. For clustering analysis, inspired by the work of Hao-Pu Li and colleagues, this study innovatively applies the three-way clustering algorithm to analyze optimal and suboptimal intervals *(Li, 2024; Li, 2023)*. The central concept of the algorithm presented in this paper, which pertains to the selection of initial cluster centers, aims to ensure their placement within the dataset rather than at its periphery. Additionally, it strives to maintain a certain minimum separation between each pair of cluster centers. This approach serves a dual purpose: firstly, it reduces the frequency of updates to the cluster centers, and secondly, it enhances the overall performance of the clustering results. When visualizing the dataset as a spatial circle, the initial cluster centers are strategically chosen within a predefined distance from the circle's center, forming a circular region. This selection strategy endeavors to distribute the initial cluster centers across different clusters as evenly as possible.

Furthermore, to move beyond simple correlation analysis and enable practical agricultural intervention, this study innovatively applies an improved K-means three-way clustering algorithm. The role of this algorithm is to systematically partition the continuous range of ecological factors into optimal, sub-optimal, and poor intervals based on their impact on plant growth. By optimizing the selection of initial cluster centers to be centrally located and well-distributed, the algorithm enhances clustering stability and accuracy. This allows for the precise identification of ecological thresholds that promote or inhibit the growth of roots, stems, and leaves, thereby providing a scientific basis for real-time environmental regulation and artificial intervention in the cultivation of high-quality *Geoherbal C. pilosula*.

2. MATERIALS AND METHODS

2.1. Data Collection and Processing

2.1.1. Quantification of Codonopsis pilosula (Lu Dangshen) 3D Model Indicators and Measurement of Ecological Factors in Authentic Production Areas

The field experiment was conducted from March to October 2023 at the *C. pilosula* cultivation base in Shijiapo Village, Liuquan Township, Lingchuan County, Jincheng City, Shanxi Province, China. The tested plant material was identified as *Codonopsis pilosula* (Lu Dangshen) (Figure 1). The experimental design utilized an initial row spacing of 30 cm and plant spacing of 20 cm, with a planting density of 5,000 plants. The tested *C. pilosula* plants were one year old.

Nine *C. pilosula* plants with robust growth were selected from the experimental field for sampling. Morphological data of the plants were collected every 10 days. A miniature weather station was installed in the experimental field to record meteorological data, including light intensity, temperature, humidity, precipitation, wind speed, soil nitrogen, phosphorus, potassium, and pH, at one-hour intervals. Based on the growth characteristics of *C. pilosula*, the entire growth season was divided into six stages: seedling stage (May–June), rapid growth stage (mid-June to mid-October), flowering stage (July–August), vigorous root growth stage (August–September), withering stage (late October), and harvesting stage (end of October). Three-dimensional (3D) scans of the roots, stems, and leaves were conducted every 10 days to monitor their growth dynamics. By combining the field-measured phenotypic data of the plant organs, the morphological data of *C. pilosula* grown in Lingchuan were obtained across different growth stages.

Using these data *(table 1; table 2)*, a 3D model of *C. pilosula* was constructed.

(a) Photograph of a Single Codonopsis pilosula Plant

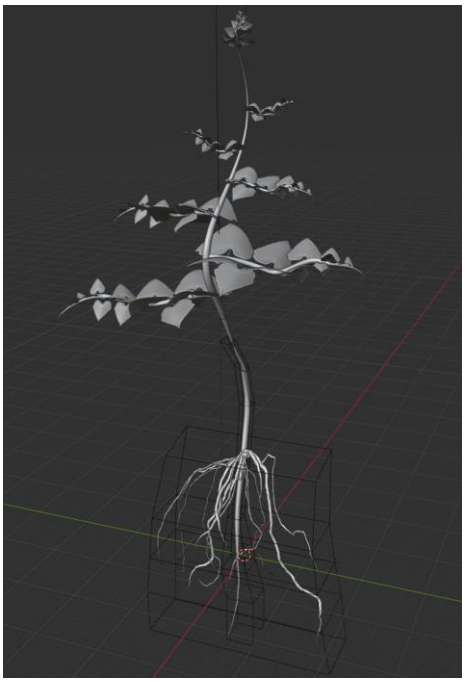

(b) 3D Dynamic Growth Model of a Single Codonopsis pilosula Plant

Fig. 1 - Image of a Single Codonopsis pilosula Plant

Table 1

Morphological Statistics of Codonopsis pilosula Organs (Partial)

Stage	Root_X1	Root_Y1	Root_Z1	Root_X2	Root_Y2	Root_Z2	Root_X3	Root_Y3	Root_Z3
Seedling Stage	0	0	0	0	-0.5	-0.3	0.1	-1	-0.6
Seedling Stage	0	0	0	0	-0.51351	-0.30541	0.1	-1.02703	-0.61081
Seedling Stage	0	0	0	0	-0.52703	-0.31081	0.1	-1.05405	-0.62162
Seedling Stage	0	0	0	0	-0.54054	-0.31622	0.1	-1.08108	-0.63243
Seedling Stage	0	0	0	0	-0.55405	-0.32162	0.1	-1.10811	-0.64324

2.1.2. Collection of Codonopsis pilosula Phenotypic Samples at Different Growth Stages

Table 2

Codonopsis pilosula Phenotypic Sample Collection at Different Growth Stages

Collection time	Lu Dangshen Picture	Notes
2023.05.20		The seedling stage of Lu Dangshen the plant is relatively short, with roots, stems, and leaves showing the same seedling stage.

Collection time	Lu Dangshen Picture	Notes
2023.06.15		The rapid growth period of Lu Dangshen medium plant height and a certain length of growth in roots, stems, and leaves.
2023.07.15		The flowering period of Lu Dangshen - the stems and leaves are too long and heavy, causing it to crawl on the ground, and the roots grow to their longest length
2023.09.05		The root system of Lu Dangshen is growing vigorously, accumulating nutrients.
2023.10.25		The withering period of Lu Dangshen the aboveground parts are gradually withering.
2023.10.28		The dormant period (harvest period) of Lu Dangshen the stems and leaves have completely dried up, leaving only the roots in the soil.

2.2. Model Construction Method

2.2.1. Development of the Codonopsis pilosula 3D Dynamic Growth Model

Using the meteorological data collected from the experimental field and the quantified phenotypic indicators derived from the 3D model of *C. pilosula*, a 3D model was developed and visualized through data analysis methods and algorithms. The three-dimensional model of *C. pilosula* established in this study is constructed using 3D scanning technology and point cloud processing techniques. The 3D dynamic growth model (3DDGM) integrates models of *C. pilosula* at various growth stages, developed through the aforementioned technologies. Correlation analysis of authentic ecological factors and phenotypic model data of *C. pilosula* at different growth stages is subsequently performed using R language, thereby establishing a comprehensive framework for understanding the relationship between ecological variables and phenotypic traits.

The 3DDGM developed in this study consists of two main modules: (i) phenotypic correlation analysis, and (ii) optimal and suboptimal interval determination. The model is based on experimental field meteorological data and the quantified 3D model indicators of *C. pilosula* phenotypes. An improved K-means three-way clustering algorithm was employed as the primary analytical method. The model uses the strength of correlations and the intervals of ecological factors that promote or inhibit plant growth as a foundational analysis to construct the 3DDGM for *C. pilosula*. Figure 2 provides an overview of the overall structure of the model. The input parameters for the 3DDGM include the quantified 3D model indicators of *C. pilosula* phenotypes and ecological factor data from the authentic production area during corresponding growth

periods. Spearman's rank correlation coefficient was applied to analyze the relationships between ecological factors and the length, diameter, and other traits of the roots, stems, and leaves. Using the improved K-means three-way clustering algorithm, ecological factors promoting and inhibiting the phenotypic traits of *C. pilosula* were classified. Finally, the results served as key references for the dynamic growth aspect of *C. pilosula*. As the growth cycle progresses, changes in ecological factors drive corresponding updates in the 3D dynamic growth model of *C. pilosula*.

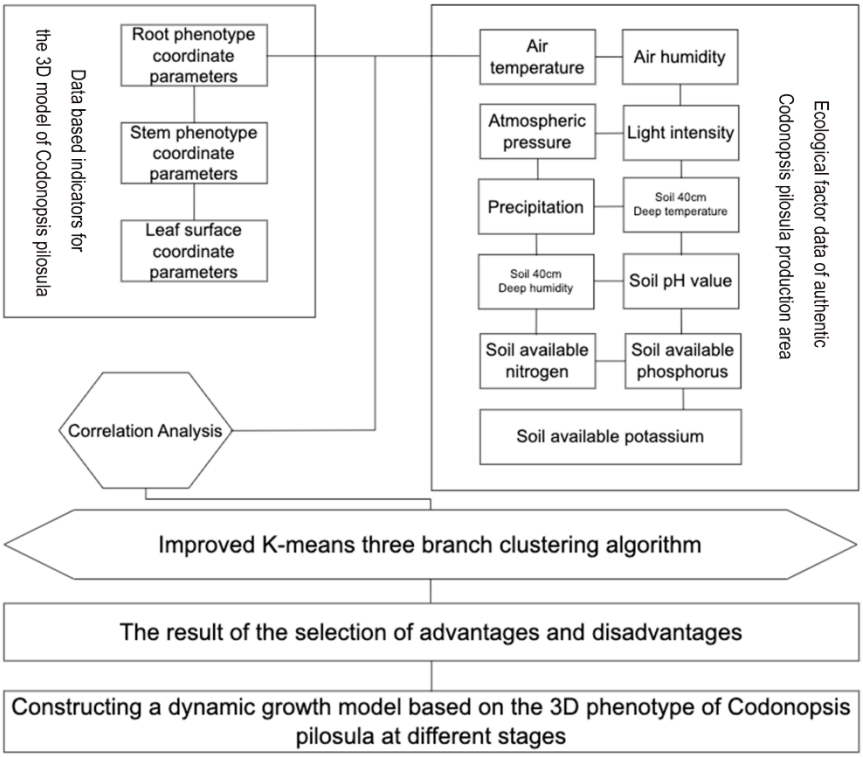

(a) Modular Functions and Technical Workflow of Codonopsis pilosula MP Model

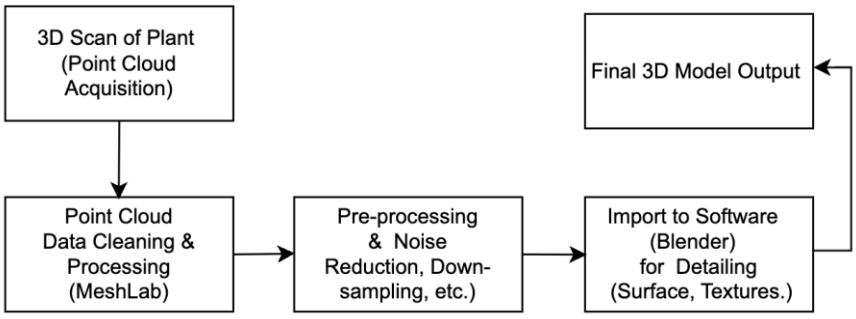

(b) The flow chart of model construction

Fig. 2 - Modular functions and technical workflow of *Codonopsis pilosula* MP model and the flow chart of model construction

2.2.2. Phenotypic Correlation Analysis

The phenotypic correlation analysis in this study was primarily based on the Spearman's Rank Correlation Coefficient, developed by Charles Spearman. For analyzing the correlation between ecological factor data from authentic *C. pilosula* production areas and the quantified indicators of the 3D model, a comparative analysis of correlation models was first conducted. Commonly used correlation coefficients for such studies include the Pearson Correlation Coefficient and the Spearman's Rank Correlation Coefficient. The Spearman's Rank Correlation Coefficient is specifically designed to handle non-linear relationships and is particularly suitable for ordinal data or data that do not follow a normal distribution. It serves as a non-parametric alternative to the Pearson Correlation Coefficient.

By contrast, the Pearson Correlation Coefficient measures the strength of linear relationships. The correlation calculation using the Pearson Correlation Coefficient is expressed in Equation (1).

$$r = \frac{n\sum x_i y_i - \sum x_i y_i}{\sqrt{(n\sum x_i^2 - (\sum x_i)^2)(n\sum y_i^2 - (\sum y_i)^2)}} \quad (1)$$

In the formula, n represents the sample size; $\sum x_i$ and $\sum y_i$ are the sums of all sample data for x and , respectively; $\sum x_i y_i$ is the sum of the products of each pair of x_i and y_i ; and $\sum x_i^2$ and $\sum y_i^2$ are the sums of the squares of x_i and y_i, respectively.

The correlation calculation using the Spearman's Rank Correlation Coefficient is expressed in Eq. (2).

$$\rho = 1 - \frac{6\sum d_i^2}{n(n^2-1)} \quad (2)$$

In the formula, ρ represents the Spearman's Rank Correlation Coefficient; di is the rank difference for each data pair (i.e., the difference between the ranks of x_i and y_i); and n is the sample size.

The rank is the assigned ordinal position of a data point within a dataset based on a specific order (typically ascending or descending). The calculation of ranks is expressed in Equation (3).

$$R = \frac{rank_1 + rank_2 + \cdots + rank_k}{k} \quad (3)$$

The calculated Spearman's Rank Correlation Coefficients (ρ) indicate the following relationships(Data display is shown in Table 3): the correlation between MAT and X18 is ρ = 0.61, and between MAT and X19 is ρ = 0.75; the correlation between AP and X17 is ρ = 0.63, and between AP and X24 is ρ = -0.75; the correlation between GHI and X19 is ρ = 0.77, and between GHI and X22 is ρ = 0.65; the correlation between ARH and X18 is ρ = 0.62, and between ARH and X22 is ρ = -0.69; the correlation between 40 cm MAT and X19 is ρ = -0.61, and between 40 cm MAT and X20 is ρ = 0.66; the correlation between DAP and X20 is ρ = 0.72, and between DAP and X23 is ρ = -0.74; the correlation between N and X21 is ρ = -0.67, and between N and X25 is ρ = 0.64; the correlation between P and X23 is ρ = 0.80, and between P and X28 is ρ = 0.81; the correlation between K and X24 is ρ = -0.71, and between K and X29 is ρ = -0.68 .

Table 3

Spearman rank correlation results

Factor 1	Factor 2	Spearman's Rank Correlation (ρ)
MAT	X18	0.61
MAT	X19	0.75
AP	X17	0.63
AP	X24	-0.75
GHI	X19	0.77
GHI	X22	0.65
ARH	X18	0.62
ARH	X22	-0.69
40 cm MAT	X19	-0.61
40 cm MAT	X20	0.66
DAP	X20	0.72
DAP	X23	-0.74
N	X21	-0.67
N	X25	0.64
P	X23	0.8
P	X28	0.81
K	X24	-0.71
K	X29	-0.68

The phenotypic correlation analysis was validated using hourly meteorological data from the field weather station at the *C. pilosula* cultivation base in Shijiapo Village, Liuquan Township, Jincheng City, Shanxi Province. These data were used to verify the correlation analysis model.

2.2.3. Optimal and Suboptimal Interval Determination

The determination of optimal and suboptimal intervals in this study was primarily based on the Improved K-means Three-Branch Clustering (IKMTBC) algorithm. Under the framework of IKMTBC, ecological factors that promote or inhibit the phenotypic growth of *C. pilosula* plants were clustered to identify the optimal intervals for different growth stages within the same growth cycle. The clustering process is expressed in Equation (4).

$$d(x_i, c_j) = \sqrt{\sum_{k=1}^{n} (x_{ik} - c_{jk})^2} \quad (4)$$

In the formula, x_i represents the feature vector of the i-th data point; c_j denotes the centroid of the j-th cluster; n is the dimension of the feature space; and $d(x_i, c_j)$ is the Euclidean distance between data point x_i and cluster center c_j.

Using this formula, it was calculated that within the positive influence interval of 40 cm MAT ranging from 15.2 to 22.5, root growth (referenced by X20) exhibited a positive correlation with a Spearman's Rank Correlation Coefficient of ρ = 0.66. Within this interval, a 5% increase in humidity corresponded to an approximate 10% increase in root growth. Similarly, nitrogen (N) within the positive influence interval of 0.6 to 8.0 showed a positive correlation with root growth (referenced by X25) with ρ = 0.64. For every 1-unit increase in soil nitrogen, root growth increased by approximately 8%. Within the positive influence interval of MAT ranging from 16.94 to 30.81, stem growth (referenced by X17 and X18) showed a positive correlation with Spearman's Rank Correlation Coefficients of ρ = 0.61 and ρ = 0.63, respectively. For every 1°C increase in temperature, stem growth increased by approximately 7%. Global Horizontal Irradiance (GHI) in the positive influence interval of 255 to 350 demonstrated a high positive correlation with stem growth (referenced by X19), with ρ = 0.77. For every 10-unit increase in light intensity, stem growth increased by approximately 12%. In the negative influence interval of ARH ranging from 50.3 to 60.9, leaf growth (referenced by X22) exhibited a negative correlation with ρ = -0.69. When humidity decreased by 5%, leaf growth increased by approximately 6%. In the positive influence interval of phosphorus (P) ranging from 1.2 to 9.8, leaf growth (referenced by X28) showed a strong positive correlation with ρ = 0.81. For every 1-unit increase in soil phosphorus, leaf growth improved by approximately 9%.

The validation of optimal and suboptimal interval determinations was conducted using hourly meteorological data from the weather station at the *C. pilosula* cultivation, in the year 2024. These data were used to verify the clustering and interval determination results.

Table 4

Equations of the Codonopsis pilosula 3D Dynamic Growth Model

Model Type	Formulas	Descriptive	
Phenotypic correlation analysis formula	$\rho = 1 - \frac{6\sum d_i^2}{n(n^2-1)}$	Spearman's rank correlation coefficient formula	ρ Spearman's rank correlation coefficient d_i The rank difference of each pair of data points (i.e.$x_i$and y_i(the difference between the ranks of the) n is the size of the sample x_i denotes the number of i Eigenvectors of the data points c_j Denotes the first j The center (center of mass) of a cluster n denotes the dimension of the feature S_j is the first j Number of data points in a cluster x_i denotes belonging to the cluster S_j of the data point
	$R = \frac{rank_1 + rank_2 + \cdots + rank_k}{k}$	Ordinal formula	
	$d_i = R_{xi} - R_{yi}$	The formula for calculating the rank difference	
	d_i^2	The formula for squaring the rank difference	
	$\sum d_i^2$	The formula for the sum of the squares of the rank differences	
Calculation formula for choosing between good and bad options	$d(x_i, c_j) = \sqrt{\sum_{k=1}^{n} (x_{ik} - c_{jk})^2}$	Distance metric formula: Euclidean distance	
	$c_j = \frac{1}{\lvert S_j \rvert} \sum_{x_i \in S_j} x_i$	Cluster center (center of mass) update formula	
	$J = \sum_{j=1}^{k} \sum_{x_i \in S_j} \lvert\lvert x_i - c_j \rvert\rvert^2$	Minimizing the squared error formula	

Model Type	Formulas	Descriptive	
	$S_j = \{x_i: \|\|x_j - c_j\|\|^2 \leq \|\|x_j - c_l\|\|^2 \forall l = 1, \ldots, k\}$	Cluster assignment rules	J is the total squared error
	$c_j^{(t+1)} = c_j^{(t)} \forall j$	convergence condition equation (math.)	k is the number of clusters (in three-branch clustering, the $k = 3$, in this study $k = 2$)

3. RESULTS AND ANALYSIS

3.1. Codonopsis pilosula 3D Point Cloud Modeling Results

The 3D point cloud was obtained through point cloud scanning, and the models were refined and completed using Meshroom and Blender. The resulting static models of *C. pilosula* at four different growth stages within a complete growth cycle are shown in Figure 3.

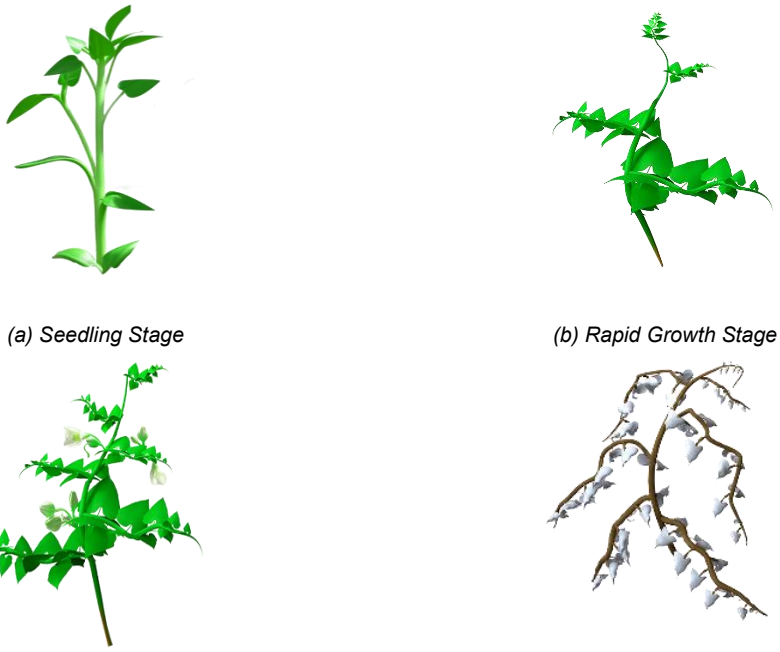

(a) Seedling Stage *(b) Rapid Growth Stage*

(c) Flowering Stage and Vigorous Root Growth Stage *(d) Withering Stage and Harvesting Stage*

Fig. 3 - Stem and Leaf Models of Codonopsis pilosula During Different Stages Within Its Growth Cycle

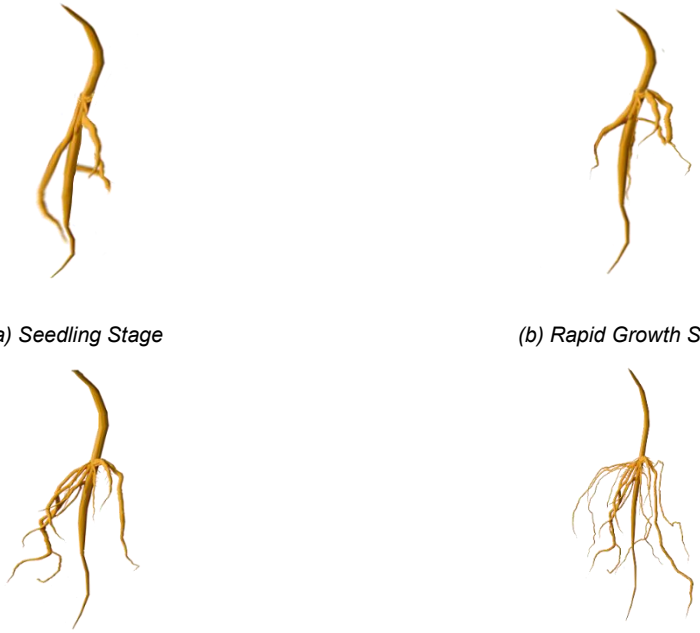

(a) Seedling Stage *(b) Rapid Growth Stage*

(c) Flowering Stage *(d) Vigorous Root Growth Stage*

(e) Withering Stage (f) Harvesting Stage

Fig. 4 - Root Models of Codonopsis pilosula at Different Stages Within Its Growth Cycle

3.2. Validation of Phenotypic Correlation Analysis Results

The phenotypic extrapolation and simulation were conducted using hourly meteorological data from the weather station at the *C. pilosula* cultivation, in the year 2024. The correlation coefficients (ρ) used as evaluation metrics for correlation analysis are presented in Tables 5, 6, and 7, while the corresponding visualizations are shown in Figures 5, 6, and 7.

The data indicate that soil moisture at a depth of 40 cm, soil pH, soil nitrogen (available nitrogen), soil phosphorus (available phosphorus), and soil potassium (available potassium) exhibit a strong positive correlation with root phenotypic traits (length and thickness) of *C. pilosula*, while showing a strong negative correlation with stem (length and diameter) and leaf (area, length and width) phenotypic traits. Air humidity and precipitation were found to have a statistically insignificant impact on the phenotypic traits of the roots, stems, and leaves. Atmospheric pressure and light intensity demonstrate moderate negative correlations with root phenotypic traits (length and thickness) and moderate positive correlations with stem and leaf phenotypic traits.

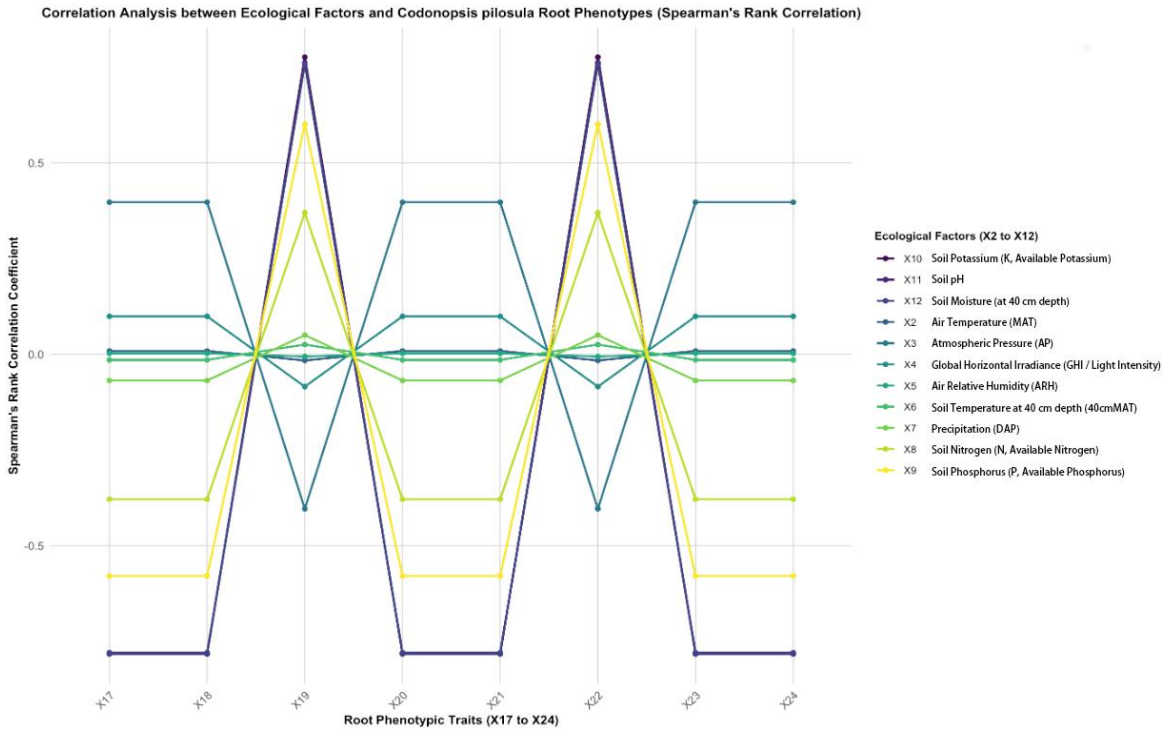

Fig. 5 - Correlation Analysis Between Ecological Factors and Root Phenotypes of Codonopsis pilosula (Spearman's Rank Correlation Coefficient)

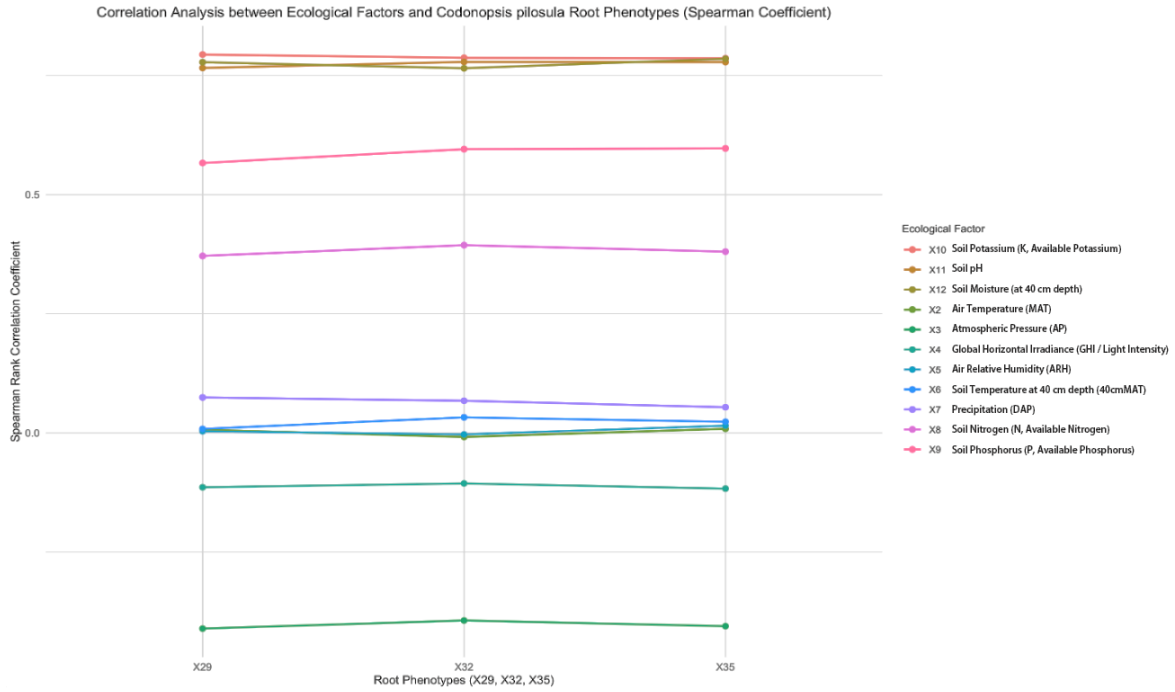

Fig. 6 - Correlation Analysis Between Ecological Factors and Stem Phenotypes of Codonopsis pilosula (Spearman's Rank Correlation Coefficient)

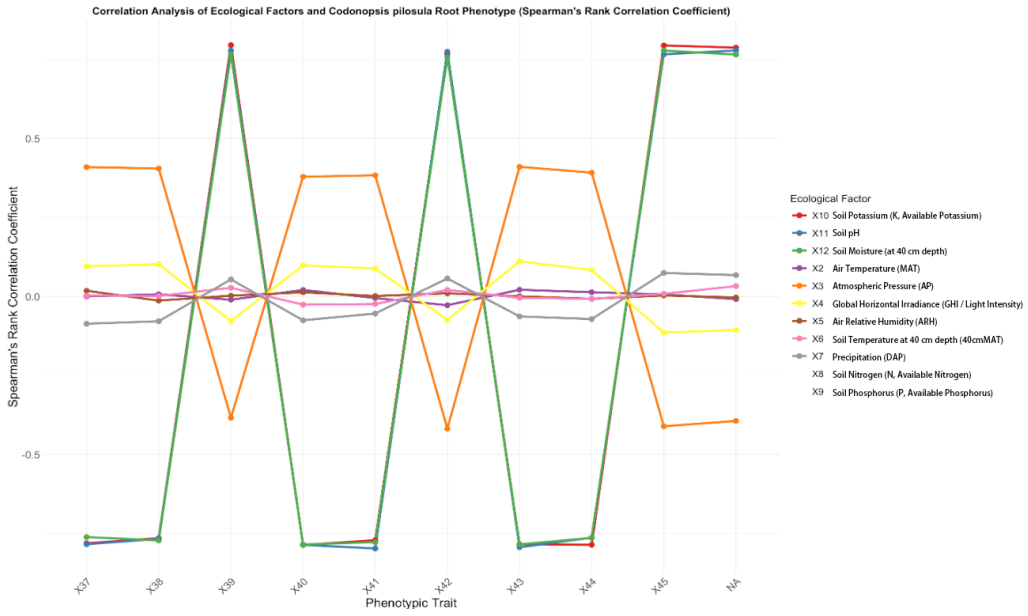

Fig. 7 - Correlation Analysis Between Ecological Factors and Leaf Phenotypes of Codonopsis pilosula (Spearman's Rank Correlation Coefficient)

Table 5

Spearman's Rank Correlation Coefficients Between Ecological Factors and Effective Root Phenotypes of Codonopsis pilosula

	X17	X18	X19	X20
X2	0.008889201	0.008889201	-0.015922468	0.008889201
X3	0.397636007	0.397636007	-0.403411035	0.397636007
X4	0.099350649	0.099350649	-0.084226082	0.099350649
X5	0.002772903	0.002772903	-0.005817188	0.002772903
X6	-0.014512989	-0.014512989	0.025762690	-0.014512989
X7	-0.068161226	-0.068161226	0.050304671	-0.068161226
X8	-0.378392610	-0.378392610	0.369886216	-0.378392610
X9	-0.578882575	-0.578882575	0.601051448	-0.578882575

	X17	X18	X19	X20
X10	-0.782679559	-0.782679559	0.776476231	-0.782679559
X11	-0.782019328	-0.782019328	0.761566939	-0.782019328
X12	-0.779272616	-0.779272616	0.758397836	-0.779272616

	X21	X22	X23	X24
X2	0.008889201	-0.015922468	0.008889201	0.008889201
X3	0.397636007	-0.403411035	0.397636007	0.397636007
X4	0.099350649	-0.084226082	0.099350649	0.099350649
X5	0.002772903	-0.005817188	0.002772903	0.002772903
X6	-0.014512989	0.025762690	-0.014512989	-0.014512989
X7	-0.068161226	0.050304671	-0.068161226	-0.068161226
X8	-0.378392610	0.369886216	-0.378392610	-0.378392610
X9	-0.578882575	0.601051448	-0.578882575	-0.578882575
X10	-0.782679559	0.776476231	-0.782679559	-0.782679559
X11	-0.782019328	0.761566939	-0.782019328	-0.782019328
X12	-0.779272616	0.758397836	-0.779272616	-0.779272616

Table 6

Spearman's Rank Correlation Coefficients Between Ecological Factors and Effective Stem Phenotypes of Codonopsis pilosula

	X29	X32	X35
X2	-0.008889201	-0.008889201	-0.008889201
X3	-0.397636007	-0.397636007	-0.397636007
X4	-0.099350649	-0.099350649	-0.099350649
X5	-0.002772903	-0.002772903	-0.002772903
X6	0.014512989	0.014512989	0.014512989
X7	0.068161226	0.068161226	0.068161226
X8	0.378392610	0.378392610	0.378392610
X9	0.578882575	0.578882575	0.578882575
X10	0.782679559	0.782679559	0.782679559
X11	0.782019328	0.782019328	0.782019328
X12	0.779272616	0.779272616	0.779272616

Table 7

Spearman's Rank Correlation Coefficients Between Ecological Factors and Effective Leaf Phenotypes of Codonopsis pilosula

	X37	X38	X39
X2	-0.008889201	-0.008889201	-0.008889201
X3	-0.397636007	-0.397636007	-0.397636007
X4	-0.099350649	-0.099350649	-0.099350649
X5	-0.002772903	-0.002772903	-0.002772903
X6	0.014512989	0.014512989	0.014512989
X7	0.068161226	0.068161226	0.068161226
X8	0.378392610	0.378392610	0.378392610
X9	0.578882575	0.578882575	0.578882575
X10	0.782679559	0.782679559	0.782679559
X11	0.782019328	0.782019328	0.782019328
X12	0.779272616	0.779272616	0.779272616

	X40	X41	X42
X2	-0.008889201	-0.008889201	-0.008889201
X3	-0.397636007	-0.397636007	-0.397636007
X4	-0.099350649	-0.099350649	-0.099350649
X5	-0.002772903	-0.002772903	-0.002772903
X6	0.014512989	0.014512989	0.014512989
X7	0.068161226	0.068161226	0.068161226
X8	0.378392610	0.378392610	0.378392610
X9	0.578882575	0.578882575	0.578882575
X10	0.782679559	0.782679559	0.782679559
X11	0.782019328	0.782019328	0.782019328
X12	0.779272616	0.779272616	0.779272616

	X43	X44	X45
X2	0.007702614	-0.008889201	-0.008889201
X3	-0.438694891	-0.397636007	-0.397636007
X4	-0.052197959	-0.099350649	-0.099350649
X5	-0.060106469	-0.002772903	-0.002772903
X6	-0.013594520	0.014512989	0.014512989
X7	0.063190961	0.068161226	0.068161226
X8	0.315077974	0.378392610	0.378392610
X9	0.551818620	0.578882575	0.578882575
X10	0.763201924	0.782679559	0.782679559
X11	0.764308913	0.782019328	0.782019328
X12	0.762254104	0.779272616	0.779272616

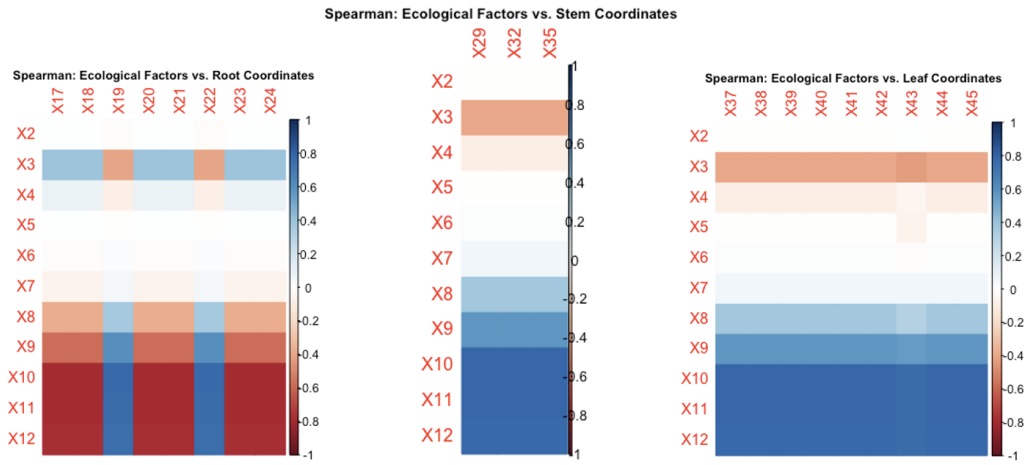

Fig. 8 - Visualization of the Correlation Analysis Between Ecological Factors and the Root Phenotype of *Codonopsis pilosula* (Spearman's Rank Correlation Coefficient: Direction and Strength of Correlation).

3.3. Validation of Optimal and Suboptimal Interval Determination Results

In this study, ecological factors that influence the phenotypic growth of *C. pilosula* were clustered to identify the optimal intervals for different growth stages within, the same plant growth and development cycle. The determination of optimal and suboptimal intervals was validated using phenotypic extrapolation and simulation results based on hourly meteorological data from the weather station at the *C. pilosula* cultivation in 2024.

The simulation results are as follows:

1. Atmospheric Temperature (MAT, °C):

• Between 16.94°C and 30.81°C, MAT positively influenced the following phenotypic traits: X17, X18, X19, X20, X21, X22, X23, X24, X29, and X32.

• Between 23.77°C and 30.81°C, MAT positively influenced the phenotypic traits X35, X37, X38, X39, X40, X41, X42, X43, X44, and X45.

2. Atmospheric Pressure (AP, hPa):

• Between 9.03 hPa and 9.53 hPa, AP negatively influenced the phenotypic traits X17, X18, X19, X20, X21, X22, X23, X24, X29, and X32.

3. Global Horizontal Irradiance (GHI, W/m²):

• Between 258.86 W/m² and 276.86 W/m², GHI positively influenced the phenotypic traits X17, X18, X19, X20, X21, X22, X23, X24, X29, and X32.

• Between 228.86 W/m² and 258.86 W/m², GHI positively influenced the phenotypic traits X35, X37, X38, X39, X40, X41, X42, X43, X44, and X45.

4. Atmospheric Humidity (ARH, %):

• Between 68.15% and 98.86%, ARH negatively influenced the phenotypic traits X17, X18, X19, X20, X21, X22, X23, X24, X29, and X32.

5. Soil Temperature at 40 cm Depth (40 cm MAT, °C):

• Between 23.59°C and 25.60°C, 40 cm MAT negatively influenced the phenotypic traits X17, X18, X19, X20, X21, X22, X23, X24, X29, and X32.

• Between 20.59°C and 23.59°C, 40 cm MAT negatively influenced the phenotypic traits X35, X37, X38, X39, X40, X41, X42, X43, X44, and X45.

6. Precipitation (DAP, mm):

• Between 0 mm and 6 mm, DAP negatively influenced the phenotypic traits X17, X18, X19, X20, X21, X22, X23, X24, X29, and X32.

• Between 28.59 mm and 30.59 mm, DAP negatively influenced the phenotypic traits X35, X37, X38, X39, X40, X41, X42, X43, X44, and X45.

7. Soil Nutrients:

• Soil Available Nitrogen (N, g/kg):

• Between 2.16 g/kg and 3.20 g/kg, N negatively influenced the phenotypic traits X17, X18, X19, X20, X21, X22, X23, X24, X29, and X32.

• Between 2.20 g/kg and 2.26 g/kg, N negatively influenced the phenotypic traits X35, X37, X38, X39, X40, X41, X42, X43, X44, and X45.

• Soil Available Phosphorus (P, g/kg):

• Between 7.56 g/kg and 8.34 g/kg, P positively influenced the phenotypic traits X17, X18, X19, X20, X21, X22, X23, X24, X29, and X32.

• Between 8.56 g/kg and 8.76 g/kg, P positively influenced the phenotypic traits X35, X37, X38, X39, X40, X41, X42, X43, X44, and X45.

• Soil Available Potassium (K, g/kg):

• Between 1 g/kg and 5 g/kg, K negatively influenced the phenotypic traits X17, X18, X19, X20, X21, X22, X23, X24, X29, and X32.

• Between 51 g/kg and 68 g/kg, K negatively influenced the phenotypic traits X35, X37, X38, X39, X40, X41, X42, X43, X44, and X45.

The validation results confirmed that the simulation outcomes closely matched the observed patterns of phenotypic variation induced by changes in ecological factors throughout the growth cycle of *C. pilosula*. This demonstrates that the study effectively captures the dynamic phenotypic changes across different growth stages, validating the robustness and accuracy of the optimal and suboptimal interval determination.

4. DISCUSSION

This study successfully achieved full-cycle 3D dynamic modeling of *C. pilosula* growth by conducting 3D modeling, analyzing the correlation between ecological factors (MAT, AP, GHI, ARH, 40 cm MAT, DAP, N, P, K, soil PH and soil moisture) and phenotypes, and determining the optimal intervals for the influence of ecological factors on phenotypic traits (stem, root and leaf phenotypic traits). Although earlier works from the 1970s and subsequent research proposed methods such as the Lindenmayer System (L-system) and Reference Axis Technique to describe plant 3D structures, these approaches have seen limited application in

studies of Chinese geoherbal plants. To address this gap, this study utilized basic 3D scanning and point cloud reconstruction techniques alongside related model repair and rendering methods to reconstruct the 3D phenotype of *C. pilosula*. Static 3D models, particularly for *C. pilosula* and other Chinese geoherbal plants, offer limited functionality in verifying geoherbal authenticity and quality. Therefore, this study proposed a 3D dynamic model to reflect the phenotypic variations of *C. pilosula*, thereby indirectly representing its geoherbal authenticity and quality. In terms of correlation analysis between ecological factors and *C. pilosula* phenotypic parameters, Pearson introduced the Pearson product-moment correlation coefficient in 1895, and Spearman introduced the Spearman's rank correlation coefficient in 1904. However, considering the non-linear nature of the data observed over the full growth cycle and the applicability of non-linear correlation methods, this study employed Spearman's rank correlation coefficient to assess the strength and direction of the influence of ecological factors on *C. pilosula* phenotypic traits. During the experimental validation, the Spearman's rank correlation coefficient used to analyze the relationship between *C. pilosula* phenotypic data and geoherbal ecological factor data showed a slight deviation of approximately 2% (Figure 7). This discrepancy likely stems from variations in phenotypic data caused by annual differences in ecological factors at the geoherbal production site, even though the overall growth trends within each cycle remained consistent. These variations introduced fluctuations in the analysis results. For optimal and suboptimal interval determination, this study was inspired by the application of the K-means three-way clustering algorithm in optimal threshold control for pigsty temperature regulation by Hao-Pu Li et al *(Li, 2023)*. The methodology was adapted and improved to control ecological factors influencing *C. pilosula* growth. This approach not only enhances geoherbal authenticity and quality but also significantly reduces the challenges of cultivating geoherbal plants in non-native environments. Using this interval determination method, the study demonstrated significant positive or negative effects of ecological factors within specific ranges on the phenotypic traits of *C. pilosula*. For example, atmospheric temperature (MAT) within the range of 16.94 ℃ to 30.81 ℃ had the most substantial positive effect on certain phenotypic traits, whereas atmospheric pressure (AP) within the range of 9.033 hPa to 9.533 hPa had the greatest negative effect on corresponding traits. Similarly, other factors, such as global horizontal irradiance (GHI) and atmospheric humidity (ARH), exhibited their strongest regulatory effects-either positive or negative-on phenotypic traits within their respective optimal ranges. These identified optimal intervals provide a basis for further optimization of growth environments.

Compared with existing studies, this research expands upon earlier work such as that by Hu Jiadong et al., which investigated the effects of nitrogen, phosphorus, and potassium fertilizers on *C. pilosula* and determined optimal fertilization levels *(HU, 2019)*. Their study focused exclusively on the ecological factors affecting the underground parts of the plant. However, plant physiology demonstrates that the growth and development of plants in general, require a comprehensive consideration of ecological factors, including those affecting both the underground and atmospheric environments. Similarly, the study by Zixia Wang et al. used the MaxEnt model to analyze the environmental factors influencing the quality of *C. pilosula* based on integrated functional factors. While their consideration of ecological factors was thorough, applying these findings across the entire plant growth cycle would significantly enhance the practical value of their research *(Wang, 2023)*. Recognizing these gaps, our team carefully summarized and planned this study to deepen the understanding of medicinal plants, achieving relatively accurate results. However, certain limitations remain. For instance, this research primarily focuses on the relationship between ecological factors and the phenotypic traits of *C. pilosula*, without addressing the complex biochemical structures within the plant.

Compared with previous scholars research on Lu Dangshen, this study provides critical insights into the optimal ecological factor ranges for *C. pilosula*, by employing a 3D dynamic growth model (3DDGM) and correlating it with ecological variables. The results have significant implications for optimizing cultivation conditions, which could enhance both the quality and yield of *C. pilosula*. These findings are not only crucial for local cultivation strategies but also contribute to the broader understanding of cultivating other medicinal plants with similar ecological needs.

While previous research on *C. pilosula* and other medicinal plants has often focused on isolated ecological factors or applied traditional statistical approaches, this study advances the field by integrating a 3D dynamic growth model and multi-factor analysis. The incorporation of such innovative methodologies allows for a more accurate and holistic understanding of plant growth dynamics and their interaction with ecological variables, thus overcoming the limitations of earlier studies, which were unable to account for the complex interactions between plants and their environment over time. In contrast to previous studies that may have emphasized linear or static relationships, this research offers a dynamic model that tracks plant growth across different

stages and quantitatively relates ecological conditions to phenotypic traits. By leveraging advanced 3D scanning and point cloud reconstruction technologies, this study fills a gap in the existing literature by offering new methodologies for modeling plant phenotypes. Furthermore, the results establish a solid scientific foundation for optimizing *C. pilosula* cultivation practices, paving the way for enhanced agricultural sustainability and the improvement of product quality.

5. CONCLUSIONS

This study is structured around three main components:

1. Successful Construction of a 3D Model for *Codonopsis pilosula*

A comprehensive 3D dynamic growth model for *C. pilosula* was successfully developed, providing an accurate and intuitive tool for monitoring growth and assessing the quality of geoherbal plants. Phenotypic Correlation Analysis Using Spearman's Rank Correlation Coefficient

By employing Spearman's rank correlation coefficient, this study revealed the degree to which various ecological factors influence the growth of different plant parts of *C. pilosula*. Overall, ecological factors demonstrated an impact on root phenotypic traits compared to stems and leaves. Key correlations include:

- MAT: ρ = 0.61 with X18, ρ = 0.75 with X19.
- AP: ρ = 0.63 with X17, ρ = -0.75 with X24.
- GHI: ρ = 0.77 with X19, ρ = 0.65 with X22.
- ARH: ρ = 0.62 with X18, ρ = -0.69 with X22.
- 40 cm MAT: ρ = -0.61 with X19, ρ = 0.66 with X20.
- DAP: ρ = 0.72 with X20, ρ = -0.74 with X23.
- N: ρ = -0.67 with X21, ρ = 0.64 with X25.
- P: ρ = 0.80 with X23, ρ = 0.81 with X28.
- K: ρ = -0.71 with X24, ρ = -0.68 with X29.

The frequency of Spearman's rank correlation coefficients exceeding 0.6 was notably higher for roots than for stems and leaves, indicating that ecological factors play a critical role in determining geoherbal authenticity and quality. Specifically, appropriate ranges of atmospheric pressure, light intensity, soil moisture at 40 cm depth, soil pH, available nitrogen, phosphorus, and potassium significantly affected root traits such as length and thickness. Similarly, stems and leaves, which interact with atmospheric ecological factors, are also vital in influencing the quality of *C. pilosula*. While air humidity and precipitation had minimal effects on phenotypic traits, these effects remained within acceptable thresholds. Using data analysis, mathematical computations, 3D point cloud technology, and model processing methods, this study successfully reconstructed a 3D model of *C. pilosula* and employed correlation analysis and the K-means three-way clustering algorithm to establish a 3D dynamic growth model. This approach effectively reflected phenotypic changes during different growth stages.

2. Determination of optimal ecological factor intervals using three-way K-means clustering

The study identified optimal intervals for ecological factors that influence *C. pilosula* phenotypic traits:

- 40 cm MAT (15.2–22.5): A 5% increase in humidity corresponded to a 10% increase in root growth.
- N (0.6–8.0): Each 1-unit increase in available nitrogen resulted in an 8% increase in root growth.
- MAT (16.94–30.81): Each 1°C rise in temperature increased stem growth by approximately 7%.
- GHI (255–350): A 10-unit increase in light intensity increased stem growth by 12%.
- ARH (50.3–60.9): A 5% decrease in humidity increased leaf growth by approximately 6%.
- P (1.2–9.8): Each 1-unit increase in available phosphorus improved leaf growth by 9%.

These results provide scientific guidance for optimizing growth environments, enabling precise regulation of cultivation conditions and supporting the cultivation of other crops and plants.

REFERENCES

[1] Akhtar, M. S., Zafar, Z., Nawaz, R., & Fraz, M. M. (2024). Unlocking plant secrets: A systematic review of 3D imaging in plant phenotyping techniques. *Computers and Electronics in Agriculture*, 222, 109033. http://doi.org/10.1016/j.compag.2024.109033

[2] Arshad, M. A., Jubery, T., Afful, J., Jignasu, A., Balu, A., Ganapathysubramanian, B., Sarkar, S., & Krishnamurthy, A. (2024). Evaluating Neural Radiance Fields for 3D Plant Geometry Reconstruction in Field Conditions. *Plant Phenomics*, 6, 235. http://doi.org/10.34133/plantphenomics.0235

[3] Chen, H., Liu, S., Wang, C., Wang, C., Gong, K., Li, Y., Lan, Y. (2023). Point Cloud Completion of Plant Leaves under Occlusion Conditions Based on Deep Learning. *Plant Phenomics*, 5, 117. doi: https://doi.org/10.34133/plantphenomics.0117

[4] Chen, Q., Huang, S., Liu, S., Zhong, M., Zhang, G., Song, L., Zhang, X., Zhang, J., Wu, K., Ye, Z., & Kong, D. (2024). Multi-view 3D reconstruction of seedling using 2D image contour. *Biosystems Engineering*, 243, 130-147. http://doi.org/10.1016/j.biosystemseng.2024.05.011

[5] Clark, R. T., MacCurdy, R. B., Jung, J. K., Shaff, J. E., McCouch, S. R., Aneshansley, D. J., & Kochian, L. V. (2011). Three-Dimensional Root Phenotyping with a Novel Imaging and Software Platform. *Plant Physiology*, 156(2), 455-465. http://doi.org/10.1104/pp.110.169102

[6] Deng, S. J. S. Z. (2024). A Hybrid Method for Individual Tree Detection in Broadleaf Forests Based on UAV-LiDAR Data and Multistage 3D Structure Analysis. *Forests*, 15(6), 1043. http://doi.org/10.3390/f15061043

[7] Diggle, A. J. (1988). ROOTMAP-a model in three-dimensional coordinates of the growth and structure of fibrous root systems. *Plant and Soil*, 105(2), 169-178. http://doi.org/10.1007/BF02376780

[8] Gairola, S., Shariff, N., Bhatt, A., & Kala, C. P. (2010). Influence of climate change on production of secondary chemicals in high altitude medicinal plants: Issues needs immediate attention. *Journal of Medicinal Plants Research*, 4, 1825-1829.

[9] Guo, Q. Y. Z. W. (2022). An Improved Three-Way K-Means Algorithm by Optimizing Cluster Centers. *Symmetry*, 14(9), 1821. http://doi.org/10.3390/sym14091821

[10] Hu Jia-dong, Wu Zi-ding, Liu Zi-zhe, LI Wen-jun, Wang Er-huan, Liang Zong-suo, Dong Juan-e. (2019). Effects and optimum rate of nitrogen, phosphorus and potassium fertilization for Codonopsis pilosula [J]. *Journal of Plant Nutrition and Fertilizers*, 25(9): 1615-1622. DOI: 10.11674/zwyf.18369

[11] Jiang, C., Li, Z., & Yao, J. (2022). A shadowed set-based three-way clustering ensemble approach. *International Journal of Machine Learning and Cybernetics*, 13(9), 2545-2558. http://doi.org/10.1007/s13042-022-01543-5

[12] Koch, T. A. P. D. (2024). From Field to Model: Determining EROSION 3D Model Parameters for the Emerging Biomass Plant Silphium perfoliatum L. to Predict Effects on Water Erosion Processes. *Agronomy*, 14(9), 2097. http://doi.org/10.3390/agronomy14092097

[13] Latt, Z. Z., & Wittenberg, H. (2014). Improving Flood Forecasting in a Developing Country: A Comparative Study of Stepwise Multiple Linear Regression and Artificial Neural Network. *Water Resources Management*, 28(8), 2109-2128. http://doi.org/10.1007/s11269-014-0600-8

[14] Li, H. L. B. L. (2024). Three-Way k-Means Model: Dynamic Optimal Sensor Placement for Efficient Environment Monitoring in Pig House. *Animals*, 14(3), 485. http://doi.org/10.3390/ani14030485

[15] Li, H. L. H. L. (2023). Smart Temperature and Humidity Control in Pig House by Improved Three-Way K-Means. *Agriculture*, 13(10), 2020. http://doi.org/10.3390/agriculture13102020

[16] Li, H., Li, H., Li, B., Shao, J., Song, Y., & Liu, Z. (2023). Smart Temperature and Humidity Control in Pig House by Improved Three-Way K-Means. *Agriculture*, 13(10), 2020. https://doi.org/10.3390/agriculture13102020

[17] Liang, Y., Zhou, K., & Cao, L. (2024). An advanced three-dimensional phenotypic measurement approach for extracting Ginkgo root structural parameters based on terrestrial laser scanning. *Frontiers in Plant Science*, Volume 15 - 2024

[18] Lu, J., Lankhost, J. A., Stomph, T. J., Schneider, H. M., Chen, Y., Mi, G., Yuan, L., & Evers, J. B. (2024). Root plasticity improves maize nitrogen use when nitrogen is limiting: an analysis using 3D plant modelling. *Journal of Experimental Botany*, 75(18), 5989-6005. http://doi.org/10.1093/jxb/erae298

[19] Mohan, M. S. C. A. (2017). Individual Tree Detection from Unmanned Aerial Vehicle (UAV) Derived Canopy Height Model in an Open Canopy Mixed Conifer Forest. *Forests*, 8(9), 340. http://doi.org/10.3390/f8090340

[20] Murata, H., & Noshita, K. (2024). Three-Dimensional Leaf Edge Reconstruction Combining Two- and Three-Dimensional Approaches. *Plant Phenomics*, 6, 181. http://doi.org/10.34133/plantphenomics.0181

[21] Rahimmalek, M., Heidari, E. F., Ehtemam, M. H., & Mohammadi, S. (2017). Essential oil variation in Iranian Ajowan (Trachyspermum ammi (L.) Sprague) populations collected from different geographical regions in relation to climatic factors. *Industrial Crops and Products*, 95, 591-598. http://doi.org/10.1016/j.indcrop.2016.11.017

[22] Rodriguez-Sanchez, J., Snider, J. L., Johnsen, K., & Li, C. (2024). Cotton morphological traits tracking through spatiotemporal registration of terrestrial laser scanning time-series data. *Frontiers in Plant Science*, Volume 15 - 2024

[23] Rosell, J. R., Llorens, J., Sanz, R., Arnó, J., Ribes-Dasi, M., Masip, J., Escolà, A., Camp, F., Solanelles, F., Gràcia, F., Gil, E., Val, L., Planas, S., & Palacín, J. (2009). Obtaining the three-dimensional structure of tree orchards from remote 2D terrestrial LIDAR scanning. *Agricultural and Forest Meteorology*, 149(9), 1505-1515. http://doi.org/10.1016/j.agrformet.2009.04.008

[24] Roshan, T. R., Jafari, M., Golami, M., & Kazemi, M. (2024). Evaluating geometric measurement accuracy based on 3D model reconstruction of nursery tomato plants by Agisoft photoscan software. *Computers and Electronics in Agriculture*, 221, 109000. http://doi.org/10.1016/j.compag.2024.109000

[25] Rousseeuw, P. J. (1987). Silhouettes: A graphical aid to the interpretation and validation of cluster analysis. *Journal of Computational and Applied Mathematics*, 20, 53-65. http://doi.org/10.1016/0377-0427(87)90125-7

[26] Sanzo-Miró, M., Medina, A., Terry, L. A., & Alamar, M. C. (2024). Elucidating the impact of environmental factors on the growth of Colletotrichum coccodes strains isolated from potato tubers in Great Britain. *International Journal of Food Microbiology*, 423, 110843. http://doi.org/10.1016/j.ijfoodmicro.2024.110843

[27] Sun Shengxuan, Z. Y. L. S. (2024). An integrated method for phenotypic analysis of wheat based on multi-view image sequences: from seedling to grain filling stages. *Frontiers in Plant Science.* http://doi.org/10.3389/fpls.2024.1459968

[28] Tapia-Zapata, N., Saha, K. K., Tsoulias, N., & Zude-Sasse, M. (2024). A geometric modelling approach to estimate apple fruit size by means of LiDAR 3D point clouds. *International Journal of Food Properties*, 27(1), 566-583. http://doi.org/10.1080/10942912.2024.2330494

[29] Vanrell, M. A. N. L. (2024). Ecological correlates of population genetics in Linum suffruticosum, an heterostylous polyploid and taxonomic complex endemic to the Western Mediterranean Basin. *Aob Plants,* 16(4), plae27. http://doi.org/10.1093/aobpla/plae027

[30] Wang, K. P. X. L. (2024). Automated Phenotypic Trait Extraction for Rice Plant Using Terrestrial Laser Scanning Data. *Sensors*, 24(13), 4322. http://doi.org/10.3390/s24134322

[31] Wang, Z., Jia, Y., Li, P., Tang, Z., Guo, Y., Wen, L., Hu, F. (2023). Study on environmental factors affecting the quality of codonopsis radix based on MaxEnt model and all-in-one functional factor. *Scientific Reports*, 13(1), 20726. doi: 10.1038/s41598-023-46546-6

[32] Wold, H. (1966). Estimation of principal components and related models by iterative least squares. In *P. R. Krishnaiah* (Ed.), *Multivariate analysis* (pp. 391–420). New York, NY: Academic Press.

[33] Yang, D., Yang, H., Liu, D., & Wang, X. (2024). Research on automatic 3D reconstruction of plant phenotype based on Multi-View images. *Computers and Electronics in Agriculture*, 220, 108866. https://doi.org/10.1016/j.compag.2024.108866

[34] Yang, X. X. X. Z. (2019). Identification of anthocyanin biosynthesis genes in rice pericarp using PCAMP. *Plant Biotechnology Journal*, 17(9), 1700-1702. http://doi.org/10.1111/pbi.13133